Two-dimensional electron gas at the $PbTiO_3/SrTiO_3$ interface: An *ab initio* study

Binglun Yin,[1,2] Pablo Aguado-Puente,[2,3,*] Shaoxing Qu,[1,†] and Emilio Artacho[2,3,4,5]
[1]*Department of Engineering Mechanics, Zhejiang University, 310027 Hangzhou, China*
[2]*CIC Nanogune, Tolosa Hiribidea 76, 20018 San Sebastián, Spain*
[3]*Donostia International Physics Center (DIPC), Paseo Manuel de Lardizabal 4, 20018 San Sebastián, Spain*
[4]*Theory of Condensed Matter, Cavendish Laboratory, University of Cambridge, J. J. Thomson Avenue, Cambridge CB3 0HE, United Kingdom*
[5]*Basque Foundation for Science Ikerbasque, 48011 Bilbao, Spain*

(Received 15 June 2015; revised manuscript received 18 August 2015; published 8 September 2015)

In the polar catastrophe scenario, polar discontinuity accounts for the driving force of the formation of a two-dimensional electron gas (2DEG) at the interface between polar and nonpolar insulators. In this paper, we substitute the usual, nonferroelectric, polar material with a ferroelectric thin film and use the ferroelectric polarization as the source for polar discontinuity. We use *ab initio* simulations to systematically investigate the stability, formation, and properties of the two-dimensional free-carrier gases formed in $PbTiO_3/SrTiO_3$ heterostructures under realistic mechanical and electrical boundary conditions. Above a critical thickness, the ferroelectric layers can be stabilized in the out-of-plane monodomain configuration due to the electrostatic screening provided by the free carriers. Our simulations also predict that the system can be switched between three stable configurations (polarization up, down, or zero), allowing the nonvolatile manipulation of the free-charge density and sign at the interface. Furthermore, the link between ferroelectric polarization and free-charge density demonstrated by our analysis constitutes compelling support for the polar catastrophe model that is used to rationalize the formation of 2DEG at oxide interfaces.

DOI: 10.1103/PhysRevB.92.115406 PACS number(s): 73.20.−r, 77.80.−e, 31.15.A−

I. INTRODUCTION

Today, developments in deposition techniques allow researchers to routinely grow atomically sharp interfaces between transition metal oxides, boosting research on emergent phenomena at complex oxide interfaces [1,2]. Among these phenomena, one of the most striking examples is the formation of two-dimensional electron gas (2DEG) at the interface of two band insulators, $LaAlO_3$ (LAO) and $SrTiO_3$ (STO) [3]. During the past decade, considerable research efforts have been devoted to explore the LAO/STO interface and similar systems, showing that, at oxide interfaces, 2DEG can exhibit enhanced capacitance [4], magnetism [5], superconductivity [6,7], or combinations of these properties [8,9]. The discovery of 2DEG and the possibility of its manipulation and coupling with other functional properties typical of oxide perovskites have fueled intense research activity aiming at exploiting its potential functionalities. Indeed, several potential practical applications based on 2DEG have been proposed, including field effect devices [10–14], sensors [15], and solar cells [16,17].

Despite all these efforts, the driving force for the accumulation of free charge at these interfaces and the origin of the charge itself are still controversial issues. In the polar catastrophe scenario [18], a widely acknowledged model, the driving force for the formation of 2DEG is the mismatch of formal polarizations between the constituent materials [19]. Such discontinuity has a huge electrostatic energy cost and thus triggers a series of screening mechanisms that yield the accumulation of free charge at the interface. Among the various mechanisms that have been proposed, one of the most notables is *electronic reconstruction.* According to the conventional meaning of this term in the context of polar interfaces (see Ref. [20] for example), in pristine structures (with no defects, or surface adsorbates), this mechanism consists of a charge transfer between the valence and conduction bands of the system that results in an accumulation of free carriers at the interface. In practice, this mechanism might be accompanied by alternative sources of free charge, such as defects or surface redox processes [21–23]. Nevertheless, regardless of the source of the free charge, the properties of the 2DEG can in principle be tuned by manipulating its driving force, i.e., the polar discontinuity.

The polar discontinuity can be tuned in different ways. For polar centrosymmetric materials like LAO, the polar discontinuity can be effectively changed by choosing different crystalline orientations for the interface [24], or diluting the polar material [25]. After growth, the density of charge carriers at the interface can be tuned with an external electric field [10–14]. Another interesting possibility is to couple the 2DEG with a ferroelectric material, since the spontaneous polarization of the ferroelectric material might allow the nonvolatile manipulation of the electrostatic boundary conditions of the system. This approach was demonstrated in Ref. [26], where the authors observed a nonvolatile metal-insulator transition in the LAO/STO interface after switching the spontaneous polarization of a ferroelectric layer deposited over the LAO.

A more radical alternative is to directly replace the polar material with a ferroelectric layer, where the ferroelectric polarization could constitute the source for the polar discontinuity, instead of the "built-in" polarization of a polar material such as LAO. Such a ferroelectric system would possess some advantageous properties. First, unlike in the case of LAO, the magnitude of the polar mismatch in ferroelectric interfaces can be increased or decreased, and even the sign of the discontinuity might be switchable with the polarization. Second, ferroelectric thin films are typically grown at a

*p.aguado@nanogune.eu
†squ@zju.edu.cn

temperature higher than the Curie temperature, meaning that for usual materials ($BaTiO_3$, $PbTiO_3$, $PbZr_xTi_{1-x}O_3$, etc.), there is no polar discontinuity during growth, and therefore these systems should be less prone to the formation of charged defects. Of course, this scenario also presents some problems. The switchable nature of ferroelectric polarization allows the system to find alternative routes to avoid or minimize the polar catastrophe, like forming domains or stabilizing in a paraelectric phase.

The possibility of a 2DEG at ferroelectric interfaces has been recently explored using first-principles calculations and phenomenological models. Simulations of symmetric $KNbO_3/ATiO_3$ (A = Sr, Ba, Pb) superlattices suggested that indeed the properties of 2DEG formed at ferroelectric interfaces can be modulated with polarization [27]. Nevertheless, the $KNbO_3$ layers used in that paper were not stoichiometric, and thus the superlattices were metallic by construction (intrinsic doping). Therefore, no conclusion about the stability of the 2DEG itself could be extracted from those results.

Very recently, two independent papers have provided strong arguments supporting the possibility of a 2DEG spontaneously forming to screen the depolarizing field in ferroelectric thin films and its subsequent manipulation through its coupling with the polarization. *Ab initio* simulations of $BaTiO_3$/STO/$BaTiO_3$ slabs have revealed that 10-unit-cell-thick $BaTiO_3$ layers can sustain a monodomain polarization with free carriers appearing at the surface and interface [28]. However, this monodomain state was only found in one combination of polarization direction (pointing towards the interface) and surface termination (TiO_2-terminated), while all other configurations turned out to be paraelectric and insulating after ionic relaxation. In another independent study, a Landau-based model was used to discuss the stabilization of a monodomain ferroelectric phase thanks to the screening provided by a 2DEG spontaneously formed after an electronic reconstruction [29]. As in the case of the LAO/STO interface, the 2DEG (and consequently the monodomain ferroelectricity) only becomes stable above a critical thickness of the ferroelectric layer, which depends on the energetics associated with the mechanism that provides the free charge. The model even suggested that in the appropriate conditions, the monodomain polarization screened by a 2DEG might be more stable than the polydomain one. Indeed, in experiments, monodomain polarization is routinely observed in ferroelectric thin films on insulating substrates [30–35]. Such a configuration, which can only be stable if the free charge accumulates at the interfaces, together with the two previously mentioned theoretical papers provide a strong motivation to further investigate and characterize these systems.

Here, we perform first-principles simulations systematically to analyze the formation of two-dimensional (2D) electron and hole gases in a prototypical ferroelectric interface, $PbTiO_3/SrTiO_3$ (PTO/STO), under realistic mechanical and electrical boundary conditions. We investigate the transition with thickness from paraelectric to a tristable regime in which two polar (and metallic) and one nonpolar (and insulating) configurations are accessible. The properties of the stable monodomain structure and the 2D free-carrier gases are investigated, providing a detailed analysis of the free-charge distribution.

II. METHODOLOGY

We carried out simulations of PTO/STO heterostructures using the formalism of the density functional theory as implemented in the SIESTA method [36]. Exchange and correlation were treated within the local density approximation. Core electrons were replaced by *ab initio* norm-conserving, fully separable [37], Troullier-Martin pseudopotentials [38]. For Pb atoms, the scalar relativistic pseudopotential was generated using the reference configuration $6s^2$, $6p^2$, $5d^{10}$, and $5f^0$ with cutoff radii of 2.0, 2.3, 2.0, and 1.5 atomic units, respectively. In SIESTA, the one-electron eigenstates are expanded in a set of numerical atomic orbitals. The Pb basis set included a single-ζ basis set for the semicore $5d$ orbitals, a double ζ for the valence $6s$ and $6p$ orbitals, and a single ζ for two extra $6d$ and $5f$ polarization functions. The details about the pseudopotential and basis set of the rest of the atoms can be found elsewhere [39]. A Fermi-Dirac distribution with a temperature of 100 K (~ 8.6 meV) was used to smear the occupancy of the one-particle electronic eigenstates. Reciprocal space integrations were performed on a Monkhorst-Pack [40,41] k-point mesh equivalent to $6 \times 6 \times 6$ in a five-atom perovskite unit cell, while for real space integrations, a uniform grid with an equivalent plane-wave cutoff of 600 Ry was used.

In this paper, the in-plane lattice constant in all calculations was fixed to that of the fully relaxed cubic STO in bulk, i.e., $a = 3.874$ Å, to implicitly simulate the mechanical constraint imposed by the substrate. In constrained bulk PTO, the out-of-plane lattice constant is found to be $c = 4.03$ Å, with a spontaneous polarization $P_S = 0.771\ \mathrm{C/m^2}$. Note that P_S here is obtained using the corrected Born effective charge method [42], which is the first-order approximation of the total polarization (both ionic and electronic contributions). The polarization obtained with this method is a good approximation to the exact value provided by the Berry phase formalism ($0.776\ \mathrm{C/m^2}$).

For the PTO/STO heterostructures, the slab geometry with a generic formula SrO-(TiO_2-SrO)$_6$-(TiO_2-PbO)$_m$-vacuum was used, where m is the thickness of the PTO layer, and the vacuum thickness was set to approximately 50 Å. Here, the substrate consisting of 6 unit cells of STO was found to be thick enough, since the calculation with a thicker one (12 unit cells) yielded similar results (see Appendix A for further details). The dipole correction was used in all heterostructure calculations to avoid a spurious electric field due to the periodic boundary conditions. For the geometry optimization, the bottom three monolayers (7 atoms) of STO were fixed to the bulk structure to mimic the presence of a semi-infinite substrate. The out-of-plane atomic coordinates of the rest of the atoms were relaxed until the maximum force was less than $0.025\ \mathrm{eV/Å}$.

III. RESULTS

A. Frozen-phonon calculation

In order to start the geometry optimizations with reasonable structures, we followed the rationale of the phenomenological model presented in Ref. [29] to predict the critical thickness m_0 for the stable ferroelectric configuration. According to Ref. [29], the free energy per unit area of a ferroelectric thin film in open boundary conditions can be expressed as

$$G = \frac{d}{2\varepsilon_0 \chi_\eta}\left(\frac{P_\eta{}^4}{4P_S{}^2} - \frac{P_\eta{}^2}{2}\right) + \frac{d}{2\varepsilon_0\varepsilon_\infty}(\sigma - P_\eta)^2 + \Delta\sigma + \frac{\sigma^2}{2g}, \tag{1}$$

Here, d corresponds to the thickness of the ferroelectric layer (defined as $d = mc$), P_η and χ_η are the contributions of the ferroelectric soft mode to the polarization and electric susceptibility, respectively, P_S is the spontaneous polarization in bulk, ε_∞ is the background contribution of the relative permittivity [44,45], ε_0 is the vacuum permittivity, σ is the area density of free carriers, Δ is the effective band gap (that should take into account the band alignment across the interface), and g is the reduced density of states [22]. In Eq. (1), positive values of both P_η and σ are always assumed. Taking into account the electrostatic boundary conditions of the system, the total polarization of the ferroelectric layer, P, can be calculated as

$$P = \frac{P_\eta + (\varepsilon_\infty - 1)\sigma}{\varepsilon_\infty}. \tag{2}$$

Equation (1) describes the energy balance between the tendency of a ferroelectric material to develop an electric polarization [first term in the right-hand side of Eq. (1)], hindered by the interaction with a depolarizing field (second term of the equation), and the energy cost of creating free charge (which might be provided by different sources) that could partially screen the depolarizing field. The cost of forming the 2DEG is accounted for by the last two terms of Eq. (1) and comprises the energy required to promote electrons across the band gap of the system (taking into account the band alignment and other interfacial effects in the case of heterostructures) and the energy associated with the filling of the bands. A more detailed explanation about the original model can be found in Ref. [29].

According to the model, even in the absence of extrinsic screening, a metastable monodomain ferroelectric state might appear when the thickness of the ferroelectric layer d is larger than a critical value. The monodomain configuration would be accompanied by the formation of a 2D free-charge gas at the interfaces and/or surfaces of the ferroelectric material. Here, we explore the gradual emergence of the local energy minimum utilizing a frozen-phonon method within the *ab initio* formalism. The details of the atomic structure used in our frozen-phonon calculation are depicted in Fig. 1. We construct the heterostructure by stacking m bulk unit cells of the ferroelectric material on top of 6 bulk unit cells of STO. In doing so, there is an inevitable arbitrariness in the choice of the interlayer distance at the interface. The influence of the interface construction is, according to the model, mostly through the band alignment and, therefore, the effective band gap of the system [29]. However, since the phenomenon is primarily governed by electrostatics, any reasonably realistic choice for the interface structure should yield similar qualitative results. We confirmed that, indeed, different values of the interfacial distances, l (see Fig. 1), produced similar estimations for the critical thickness m_0. In this paper, the interfacial distance l is set to be a, the lattice constant of bulk STO. Different values of the polarization in PTO layers are obtained by scaling the soft-mode distortion while keeping the lattice constants unchanged ($c_{\mathrm{STO}} = a = 3.874$ Å, $c_{\mathrm{PTO}} = c = 4.03$ Å). Throughout this paper, a polarization along the [001] axis pointing towards (away from) the STO substrate is denoted as downward (upward) polarization, has a negative (positive) value, and is labeled as $P\downarrow$ ($P\uparrow$). The calculation of the total energy per unit area G of the heterostructure as a function of polarization and PTO thickness results in the points shown in Fig. 2, where the gradual development of the "triple-well" profile with increasing thickness is clearly reproduced, indicating a critical thickness for the stable ferroelectricity of $m_0 \sim 14$ for both polarization orientations.

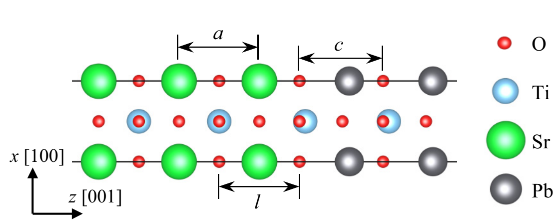

FIG. 1. (Color online) Schematic illustration of the interfacial atomic structure used in frozen-phonon calculations. In this paper, the distance l between the two oxygen atoms at the interface is set to a, the lattice constant of bulk STO.

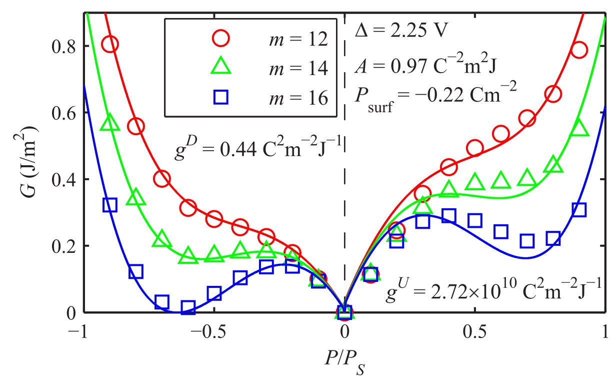

FIG. 2. (Color online) Free energy per unit area G as a function of PTO polarization for different thickness m, as calculated using the frozen-phonon method. The curves are the least-squares fitting of Eq. (3), and the obtained fitting parameters are also shown.

The energy curves obtained with the frozen-phonon methods can be compared with the predictions of the model described in Ref. [29]. As shown in Fig. 2, the frozen-phonon results display an asymmetry with respect to the polarization orientation. The model in Ref. [29] takes the same parameters for up and down polarization, but in general, real interfaces do not show that symmetry. In this case, for instance, the PTO film has a vacuum on one side and a STO substrate on the other. This asymmetry might affect the shape of the $G(P)$ curves in different ways. (i) Free surfaces of these materials tend to develop a surface dipole that modifies the polarization near the surface relative to the bulk layers in relaxed slabs [43], slightly but noticeably favoring one polarization orientation over the other. (ii) In addition to this, the interface dipole, ultimately responsible for the band alignment at the interface, is also polarization dependent, affecting the "effective band gap" entering in the model equations and altering the competition between monodomain and paraelectric configurations. Here, to account for the asymmetry of the structure and the fact that in the frozen-phonon calculations the polarization is frozen to be homogeneous throughout the ferroelectric material, we extend the original model [29] by adding new terms that phenomenologically describe the tendency to develop a surface dipole. To first order, such an effect can be described by a parabola centered at the polarization value corresponding to the surface dipole, P_{surf}, and scaling with the area (not the volume) of the system. After incorporating this correction, the free energy per unit area, G, can be expressed as

$$G = \frac{d}{2\varepsilon_0\chi_\eta}\left(\frac{{P_\eta}^4}{4{P_S}^2} - \frac{{P_\eta}^2}{2}\right) + \frac{d}{2\varepsilon_0\varepsilon_\infty}(\sigma - P_\eta)^2 + \Delta\sigma + \frac{\sigma^2}{2g} + A(P_\eta - P_{\mathrm{surf}})^2 - A{P_{\mathrm{surf}}}^2, \tag{3}$$

where A is the "stiffness" of the surface dipole. The last term of G is introduced in order to set to zero the energy reference at $P_\eta = 0$.

With the version of the model described by Eq. (3), we performed a least-squares fitting of the curves obtained with the frozen-phonon approximation. Since the analysis of the electronic structure of fully relaxed interfaces (discussed below) reveals that the band alignment of this system is quite insensitive to polarization orientation, all six curves (for both polarization orientations and different thicknesses) were fitted for the same values of Δ, A, and P_{surf}. The reduced density of states (g^D and g^U for $P\downarrow$ and $P\uparrow$, respectively) was allowed to be different for each of the two polarization directions. The rest of the parameters in Eq. (3) were fixed to the bulk PTO values as obtained from independent *ab initio* calculations, i.e., $P_S = 0.771\,\mathrm{C/m^2}$, $\chi_\eta = 26$, $\varepsilon_\infty = 7$. The least-squares fitting produced the solid curves and parameters shown in Fig. 2, demonstrating an excellent agreement between the frozen-phonon results and the model. Also, the obtained fitting parameters are all comparable to the bulk values, falling into a reasonable range for a realistic interface. The unrealistically large value of g^U produced by the fitting is attributed to the dependence of Eq. (3) on the inverse of the reduced density of states. With increasing g, the energy term associated with g goes to zero very rapidly, meaning that if g is relatively large, this energy term is negligible as compared with the rest of the contributions. In fact, for all practical purposes, a density of states larger than $\sim 2\,\mathrm{C^2m^{-2}J^{-1}}$ is indistinguishable from the limit of $g \to \infty$.

Notably, all the structures with nonzero polarization show metallic behavior, indicating that the electronic reconstruction only disappears within a tiny region around $P = 0$, a result that is also consistent with the model presented in Ref. [29].

B. Polarization profile

To confirm the stability of the polar configurations, we performed ionic relaxations for the heterostructures with m ranging from 10 to 20 unit cells for both $P\downarrow$ and $P\uparrow$, as well as those with paraelectric PTO layers. The relaxed polarization profiles with $m = 16$ are shown in Fig. 3(a), and the rest are analogous. As shown in Fig. 3(a), for $m = 16$, the two polar configurations and the nonpolar one are all stable, and the polarization in the ferroelectric phase is uniform inside PTO, with values of $-0.76P_S$ and $0.66P_S$ for downward and upward polarizations, respectively.

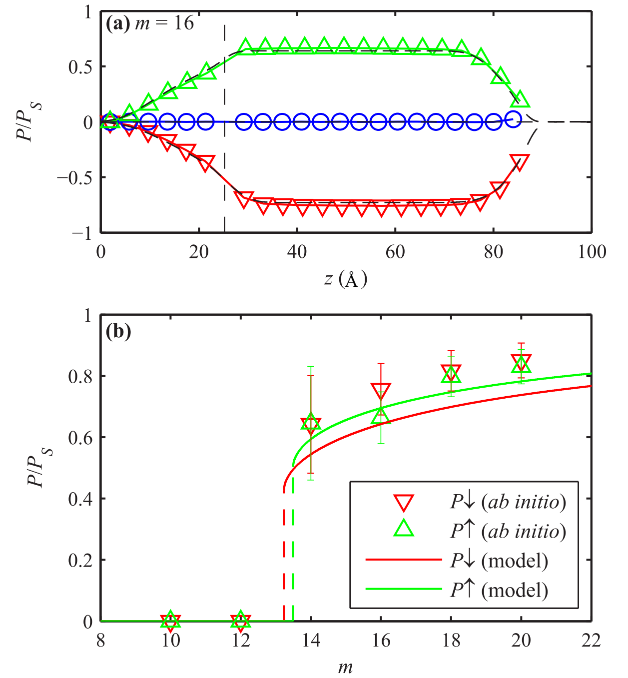

FIG. 3. (Color online) (a) Polarization as a function of z for the PTO/STO heterostructures with $m = 16$ after ionic relaxation. It is calculated by computing the dipole at each Ti-centered unit cell using the corrected Born effective charge method [42]. The system is stable in either a ferroelectric state, with downward (red) or upward (green) polarization, or in a paraelectric one (blue). The black dashed curves indicate the electric field displacement as obtained from the integration of free-carrier density. The vertical dashed line represents the position of the interfacial Ti atom in the paraelectric state. (b) The magnitude of the stable ferroelectric polarization is plotted as a function of thickness. Symbols correspond to fully relaxed structures. The continuous curves are obtained using the model described by Eq. (3) and the parameters from the fittings of Fig. 2, and not by fitting the polarization values of the relaxed structures. The error bars represent an estimation of the possible polarization fluctuations during *ab initio* calculations due to the shallowness of the ferroelectric energy minimum (details of their derivation are given in Appendix B).

The evolution of the stable polarization with thickness is depicted in Fig. 3(b) alongside two curves obtained using the model for the two polarization orientations. These two curves were calculated minimizing Eq. (3) with respect to polarization and free charge in order to obtain their equilibrium values as a function of thickness. Then, the fitting parameters obtained from the frozen-phonon calculations, shown in Fig. 2, were used to obtain the solid curves in Fig. 3(b). Figure 3(b) evidences again the good agreement between model and first-principles calculation. The curves obtained from the model slightly underestimate the polarization values obtained in the relaxed structures. The reason for this is probably the fact that in the model and the frozen-phonon calculation, the polarization is assumed to be homogeneous throughout the ferroelectric layer. As a result, the pinning of the surface dipole restrains the bulk-like region of the ferroelectric film from developing a larger value. In addition to this, in the relaxed structures, atomic distortions in the STO contribute to the screening of the free charge injected in the substrate, increasing the density of carriers that the interface can host and therefore enabling the PTO to develop a larger polarization. All these effects combined, however, give rise to a relatively small deviation from the obtained *ab initio* results of the otherwise quite adequate model.

Polarization values from *ab initio* relaxations are also susceptible to some fluctuations due to the shallowness of the energy minimum corresponding to the ferroelectric phase near the transition thickness. At the transition, the ferroelectric energy minimum becomes a saddle point, and the coordinate relaxation becomes an ill-defined problem. Away from the transition, convergence is possible, but polarization fluctuations occur for any finite threshold in the forces. In Appendix B, we derive an estimation of these fluctuations, which are represented as error bars in Fig. 3(b). The magnitude of these fluctuations is sizable near the transition but decays rapidly as the thickness increases.

The polar configurations in Fig. 3 directly demonstrate that in realistic boundary conditions, ferroelectric monodomain polarization can exist without any extrinsic screening mechanisms or polydomain formation. Furthermore, above some critical thickness m_0, the monodomain polarization can be stable in both downward and upward configurations, opening the door to a possible switching between 2DEG and 2D hole gas (2DHG) at the ferroelectric interface. It is worth pointing out that, even if for this system the critical thickness is found to be the same for both polarization orientations, this is not necessarily true in general for asymmetric heterostructures. In fact, this is most likely the reason why in a previous paper on 2DEG at ferroelectric interfaces, only one polarization orientation was found to be stable [28].

At this point, it should be noted that according to the model [29], the critical thickness for the stabilization of ferroelectricity is proportional to the band gap Δ, which is known to be severely underestimated by the local density approximation of the exchange-correlation functional. Thus, we expect that the actual transition would take place at thicknesses of the order of $\sim$30 unit cells of PTO, which is still in the range of typical values grown experimentally.

C. Free carriers

In Figs. 4(a) and 4(b), we plot the projected density of states (PDOS) of each unit-cell bilayer for the $m = 16$ interface and both polarization orientations. These figures confirm the occurrence of an electronic reconstruction, with the conduction (valence) band at the interface and the valence (conduction) band at the surface crossing the Fermi level of the heterostructure with downward (upward) polarization. Additionally, the remnant depolarization field resulting from the incomplete screening, responsible for the tilting of the bands, can also be clearly seen from the PDOS.

Furthermore, the distribution of free-charge carriers can be mapped using the local density of states (technical details can be found in the Appendix C). In Figs. 4(c) and 4(d), we plot the plane-averaged and macro-averaged [46] free-carrier density for both $P\downarrow$ and $P\uparrow$. The two profiles display similar features (with opposite sign). The sheet of free charge at the surface is strongly confined in both cases, as a consequence of the remnant depolarizing field in the ferroelectric layer. On the STO side, charge is more loosely bound to the interface by the electric field in the PTO layer and its own electrostatic interaction [47]. Therefore, it peaks near the interface and decays slowly towards the bottom surface. One detail that is worth noting is that while the 2DEG in the prototypical LAO/STO system is strictly confined to the STO side due to the band alignment between the two materials [48], here the almost vanishing band offset at the interface means that some free charge spreads into the first layers of PTO.

The free-charge profiles plotted in Figs. 4(c) and 4(d) can be integrated along z to compute the free-carrier density per unit area, labeled as σ_h and σ_e for holes and electrons, respectively. The magnitudes of σ_h and σ_e match perfectly for both polarization directions, as displayed in Figs. 4(c) and 4(d), obeying the charge neutrality. Also, they are very close to the value of the stable polarization inside the PTO layer, in agreement with the prediction of the model presented in Ref. [29]. The almost perfect overlap between polarization and interfacial free-charge values results in an excellent screening of the depolarization effects, enabling the stability of the ferroelectric phase. This result is very robust, and it displays very little sensitivity to the atomic relaxations of the STO (hosting the 2D free-charge gas at the interface) or the confinement of the free charge, as discussed in Appendix A.

Moreover, in addition to the agreement between the integral values of the free charges (σ_h and σ_e) and the polarization (P), their spatial distributions are found to match as well. This can be observed either by differentiating the polarization to obtain the bound charge profile and comparing it with the free-charge distribution [42], or, alternatively, integrating the free-charge density to obtain the electric displacement profile and comparing it with the polarization one. Taking a point in the vacuum region as one of the limits in the domain of integration (since in the vacuum region, the electric displacement $D = 0$, as guaranteed by the dipole correction), one obtains the electric displacement profiles represented as black dashed curves in Fig. 3(a). Since the difference between the polarization and the electric displacement is the electric field, the excellent overlap between the two curves throughout the whole heterostructure reflects the excellent screening provided by the electronic reconstruction. The remnant electric field inside the PTO layer can be estimated in a rather indirect way using the expression $(P - \sigma)/\varepsilon_0$ and the values listed in Figs. 4(c) and 4(d). For both polarization orientations, this calculation yields a remnant electric field of $\sim$0.2 V/Å. This value is susceptible to a large error since it is obtained from the subtraction of two very large and similar quantities. A direct estimation of the remnant depolarization field can be obtained from the macroscopic average [46] of the electrostatic potential, shown in Fig. 5, resulting in a value for the remnant electric field of $\sim$0.05 V/Å. The consistency of the electrostatic analysis constitutes strong evidence that the driving force for the electronic reconstruction is indeed the polar discontinuity, in excellent analogy with the case of the polar LAO/STO interface.

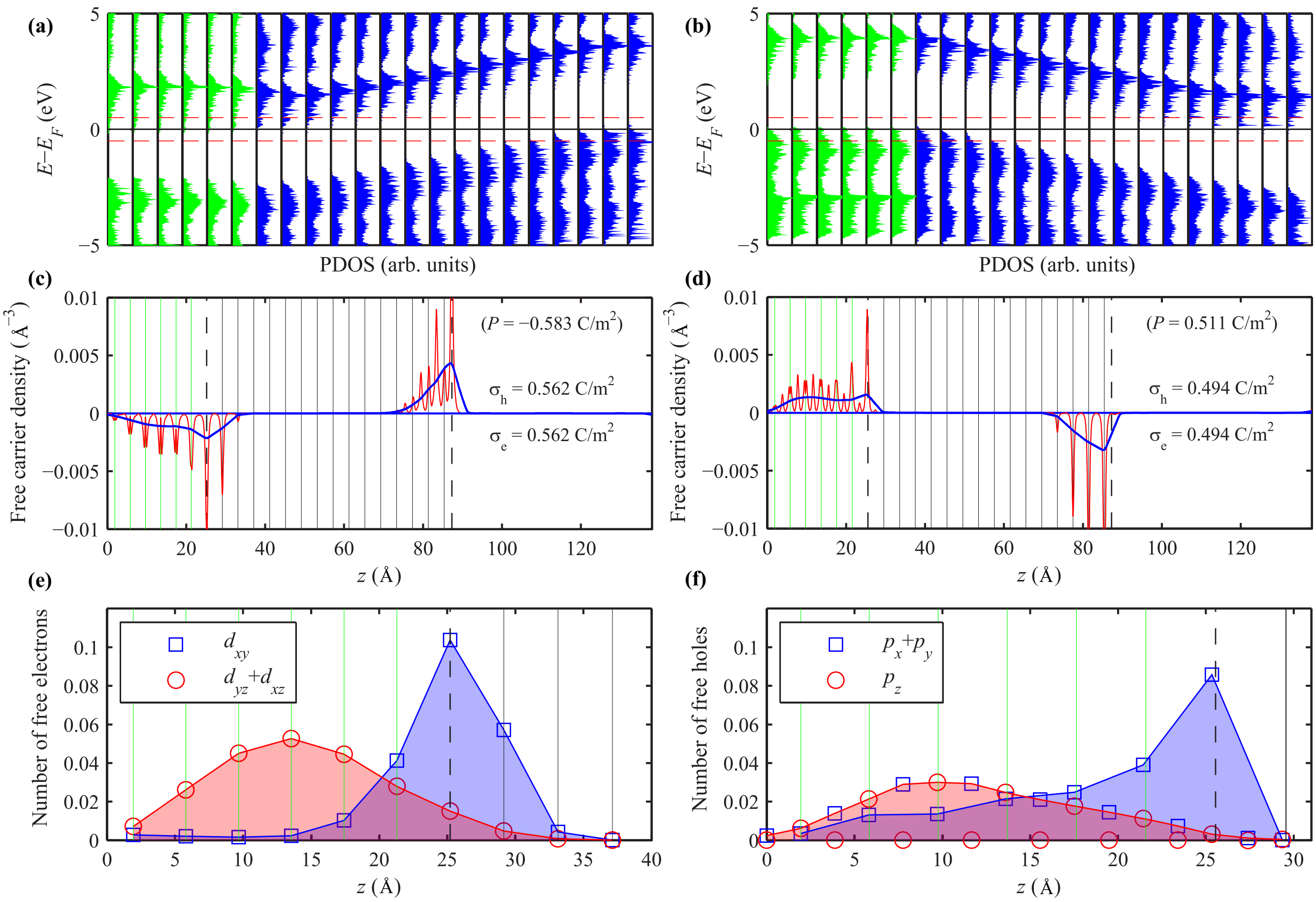

FIG. 4. (Color online) Electronic structure of the PTO/STO interface with $m = 16$ with both downward (left panels) and upward (right panels) polarizations. The bilayer-resolved PDOS is plotted in (a) and (b), with green and blue representing STO and PTO, respectively. E_F is the Fermi energy of each structure. The red dashed lines indicate the energy window used in the free-carrier density mapping (see Appendix C). In (c) and (d), plane-averaged (red) and macroscopically averaged [46] (blue) profiles of free charge are plotted, with the positive and negative values representing the free holes and free electrons, respectively. Free-carrier densities in STO are further resolved into orbital populations as shown in (e) and (f). In (c)–(f), the positions of interface and surface are indicated by the thick dashed lines, while thin solid lines mark the position of every Ti atom, with green and black for those inside STO and PTO, respectively.

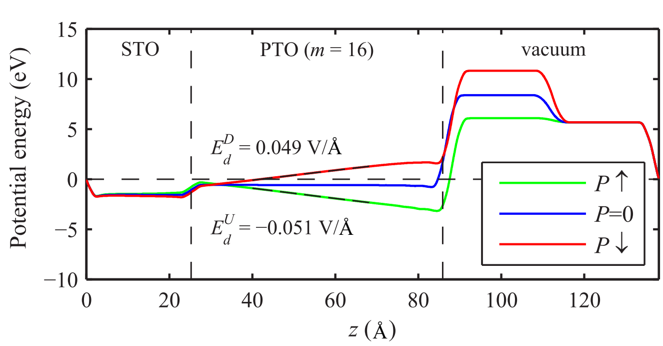

FIG. 5. (Color online) Macroscopic average [46] of the electrostatic potential energy for each polarization state in $m = 16$ heterostructures. The black dashed lines that overlap with the red and green curves indicate the linear fitting, which yields the values of the remnant depolarization field, E_d^D and E_d^U for $P\downarrow$ and $P\uparrow$, respectively.

D. 2DHG in $SrTiO_3$

It is interesting to discuss in more detail the electronic structure of the interface and, in particular, the differences between 2DEG and 2DHG, since their distinct properties might constitute a route for the design of devices in which the orientation of the polarization could be used to manipulate the transport characteristics in a nonvolatile fashion. For $P\downarrow$, a large amount of free electrons accumulates at the conduction band of STO, which means that both d_{xy} and $d_{xz} + d_{yz}$ of the Ti atoms are being partially occupied. As it was demonstrated by Popović *et al.* [49], these two sets of orbitals spread very differently from the interface in LAO/STO, an effect that, they propose, should importantly affect electronic transport in the 2DEG. The same behavior is observed here, as evidenced in Fig. 4(e).

Interestingly, here, the reversible polarization allows a similar analysis to be carried out for 2DHG. Even though a 2DHG should also form at the p-interface of a pristine LAO/STO system, the fact that it has never been observed experimentally has discouraged a deeper theoretical analysis of this system. However, since ferroelectric thin films are typically grown at temperatures higher than the Curie temperature, the electric-field-induced donor-acceptor defect pairs that are believed to be responsible for the insulating nature of the p-interface [23] are probably energetically unfavorable during the deposition of the ferroelectrics. Therefore, we propose that if a $P\uparrow$ monodomain can be condensed after growth, intrinsic electronic reconstruction or surface redox reactions are more likely to provide the necessary screening charge during the cooling process, and consequently the 2DHG might survive in these systems, as opposed to what happens in LAO/STO. Here, we take advantage of the reversible polarization to analyze in more detail the electronic structure of the interface in the presence of a 2DHG.

A decomposition of the free charge into different orbital components reveals a behavior similar to the one described in Refs. [49] and [50] for 2DEG, in which O $2p$ orbitals form two sets of bands that behave similarly to the split t_{2g} orbitals in 2DEG. By examining every individual O atom in STO, we find that all $2p$ orbitals along Ti-O bonds are fully occupied (no holes). The same feature has just been reported recently for doped STO in the bulk [51]. Then we decompose the PDOS corresponding to the 2DHG into the p_z and $p_x + p_y$ contributions in Fig. 4(f), where the points can be more easily interpreted by classifying them into three groups: (i) The population of the bands with p_z character from the SrO planes is zero, since they are along the Ti-O bonds; (ii) the bands with character p_z from TiO_2 and $p_x + p_y$ from SrO behave similarly, with both populations peaking inside STO (red shadow), just like the free electrons in $d_{xz} + d_{yz}$ orbitals in Fig. 4(e); and (iii) the population of the $p_x + p_y$ bands in TiO_2 atomic planes peaks at the interface (blue shadow), in correspondence with d_{xy} in Fig. 4(e) (note that in this case, for every O atom, either p_x or p_y is full, since it lies along the Ti-O bond). According to this, the orbital distribution in 2DHG that forms in the $P\uparrow$ case bears a strong resemblance with the one of 2DEG, i.e., a very localized band right at the interface (Ti d_{xy} for 2DEG, TiO_2 $p_x + p_y$ for 2DHG) and a long tail formed by bands with a different character (Ti $d_{xz} + d_{yz}$ for 2DEG, TiO_2 p_z and SrO $p_x + p_y$ for 2DHG).

These observations can be used to formulate a set of rules that determine the free-charge distribution in these systems and reveal the origin of the common features shared by 2DEG and 2DHG. As it was already discussed in Refs. [49] and [50], the splitting of the t_{2g} levels of Ti atoms near the interface leads to a clear differentiation between the electronic population of two sets of bands. In those papers, the analysis focused on the conduction band of STO, and it was found that the d_{xy} orbitals form bands with very small hopping along z and, therefore, a strong 2D localization. The other set of bands, which contributes to the charge spreading along z, is formed by the linear combination of d_{xz} and d_{yz} orbitals from different Ti layers. Interestingly, this behavior can also be inferred from the band structure of bulk STO. In the bulk, even if degenerated at the bottom of the conduction band (located at Γ), d_{xz} and d_{yz} on one hand and d_{xy} on the other form two separate bands when looking at the dispersion along z. The negligible dispersion of the d_{xy} band along z hints at the lack of mixing between different Ti layers at the interface. This strong 2D localization implies a strong sensitivity to the local electrostatic potential and a shift of the bands with z, as observed in Refs. [49] and [50]. Instead, the delocalization of the $d_{xz} + d_{yz}$ bands gives rise to extended bands at the interface, which are less sensitive to the potential well that confines the 2DEG.

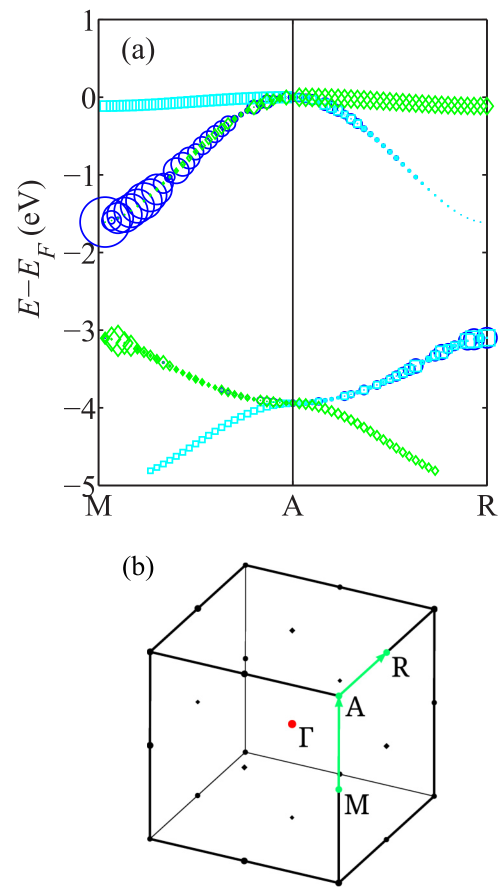

FIG. 6. (Color online) (a) Dispersion of the valence bands in STO decomposed into contributions from the different O $2p$ orbitals: p_x of SrO planes in blue circles, p_x of TiO_2 planes in cyan squares, and p_z of TiO_2 planes in green diamonds. The size of the symbols represents the weight of each orbital in the corresponding eigenstate. E_F is the Fermi energy of bulk STO. In (b), the k-point path in the tetragonal Brillouin zone is depicted. Even if STO is cubic in the bulk, here we chose to plot the tetragonal representation to illustrate the interface-induced symmetry breaking between z and in-plane (x or y) directions.

A parallel argument can be made for the charge distribution in 2DHG. As shown in Fig. 6(a), the bands at the top of the valence band can be classified into two categories: a band localized along z formed by nonbonding oxygen $p_x + p_y$ orbitals at TiO_2 planes and another one, dispersive along z, formed by $p_x + p_y$ at SrO planes and p_z at TiO_2 planes. This decomposition coincides with the different populations seen in the analysis of the free-charge profiles, and it is in agreement with the interpretation given for the population distribution in the 2DEG. The definite confirmation that the argument about band localization explains the population distribution is found by observing the electronic structure of the interface. In Fig. 7, the electronic bands near the Fermi level are decomposed into contributions from different oxygen p orbitals (each one in

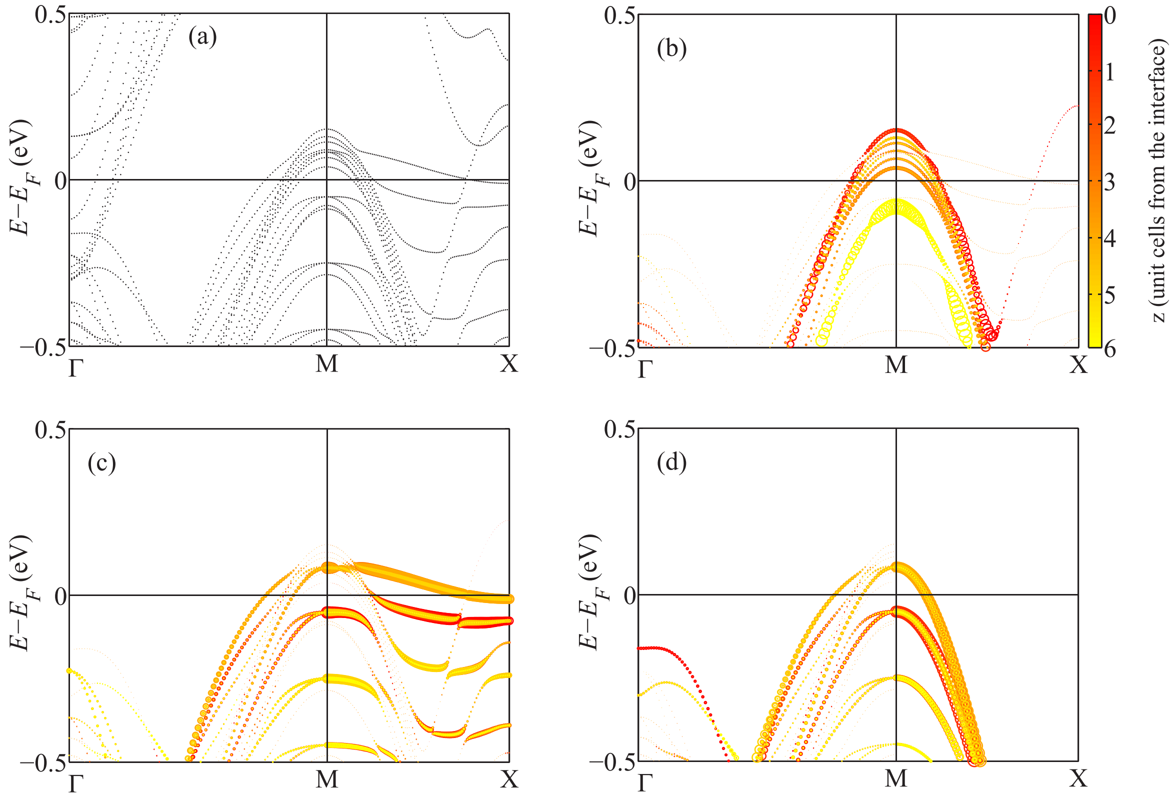

FIG. 7. (Color online) Band structure of the slab with $m = 16$ and upward polarization. (a) Electronic bands around the Fermi energy, where the top of the valence band of STO is seen crossing the Fermi level at M in the 2D Brillouin zone. Here, the k-point path from M to X corresponds to the projection of the path A to R in Fig. 6(b) onto the 2D Brillouin zone. The valence bands of STO are decomposed into contributions from different orbitals, with (b), (c), and (d) corresponding to the projection over nonbonding p_x and p_y orbitals in TiO_2 layers, $p_x + p_y$ in SrO layers, and p_z in TiO_2 layers, respectively. In (b)–(d), each eigenvalue $E_n(k)$ is plotted as a circle, with the size representing the weight of each oxygen p orbital, and the color indicating the distance from the interface, as illustrated by the legend in (b). E_F is the Fermi energy of the heterostructure.

a separate panel) and atomic layers (the color gradient goes from red for the TiO_2 plane at the interface to yellow for the SrO surface). This decomposition shows that there is a set of bands formed by p_x orbitals at individual TiO_2 planes that shifts considerably with z [Fig. 7(b)]. Several of these bands cross the Fermi level, but their population should decay rapidly from the interface. Then, there is essentially one band, with contributions from the rest of the nonbonding p orbitals throughout the whole STO substrate [Figs. 7(c) and 7(d)], responsible for the smoother charge profile in Fig. 4(f).

The analysis of the different charge populations just described allows us to anticipate, at least qualitatively, the electronic structure of 2DEG or 2DHG that might form at other polar interfaces from the bulk band structure of the host materials. It can be used, for instance, to estimate the effective masses of free-charge carriers in 2DHG from calculations of the bulk band structure. From the in-plane dispersion of the z-localized band, we get an effective mass of $m_x^* = m_y^* = -1.17m_e$ if calculated from bulk [cyan squares in Fig. 6(a)] and $-0.94m_e$ if calculated directly from the interface band structure. This constitutes a reasonable agreement, especially considering the difficulty involved in isolating the right band from the interface band structure. In bulk, one of the z-extended bands (blue circles) is degenerated with the z-localized one (cyan squares) in one of the in-plane directions, while the other one (green diamonds) has a much larger effective mass, as shown in Fig. 6(a). For the heavy holes of the z-extended band, the bulk and interface band structure calculations yield values of $-13m_e$ and $-12.7m_e$, respectively.

This analysis was already used to obtain the density of states used for all the calculations in Ref. [29] from the band structure of bulk PTO. The validity of the model, and the parameters used for its predictions, was confirmed after the comparison with the test-case first-principles simulation of PTO free-standing slabs [29].

IV. DISCUSSION

The first-principles study presented here only explores the competition between the monodomain phase sustained by an electronic reconstruction and a paraelectric configuration. However, in realistic experiments, additional elements might come into play. First, it is widely acknowledge that the source of the free charge accumulated at polar interfaces is at least partially provided by redox processes at either the surface, the interface, or a combination of both [22,23]. The participation of other sources of free charge could modify the balance between different phases, but it should not affect the main conclusion of this paper, i.e., the possibility of stabilizing monodomain ferroelectricity by 2D free-carrier gases. The only difference is that in that case, the effective gap Δ will encompass things like the formation energy of defects and the defect-defect interaction [29]. This means that for both electronic reconstruction and surface electrochemical processes, the phenomenology is expected to be similar, and the main quantitative difference would be the critical thickness for the stable ferroelectric phase. In fact, as mentioned above, since ferroelectric thin films are usually grown above the Curie temperature, during the deposition process there is no polarization discontinuity at the interface and therefore no electric-field-induced redox reactions. This should help interfaces and surfaces at ferroelectric thin films to be cleaner than those in the case of LAO [18], for which the polarization mismatch is present at all times. In the case of ferroelectrics, most mechanisms providing free charge should take place during the cooling of the sample, when the heterostructure is fully formed, and this probably favors intrinsic processes over extrinsic ones.

Secondly, the formation of polarization polydomains is an intrinsic screening mechanism that is always accessible in these systems and that eliminates the necessity for free-charge accumulation at the interfaces. The competition between these two screening mechanisms was analyzed in Ref. [29], demonstrating a crossover with thickness between the two configurations: polydomain for small thicknesses and monodomain with 2DEG for larger thicknesses. More importantly, the stability of monodomain ferroelectricity in PTO thin films on STO has indeed been confirmed experimentally numerous times [30–35], but in the absence of screening charge at the interface, such a configuration would be impossible according to simple electrostatic arguments. Surprisingly, the process that stabilizes monodomain ferroelectricity in such systems has received little attention in the past [52]. This paper provides a possible mechanism that would explain such observations, and it should motivate further investigation of the screening processes that take place in these systems and how one might take advantage of them to confer ferroelectric interfaces with new functionalities.

Finally, one important result of this paper is that it provides strong evidence supporting the polarization mismatch as the driving force for the formation of the 2DEG at the LAO/STO interface. This mechanism is still under debate, mostly because of the predictions from alternative interpretations that have been proposed, like intrinsic doping introduced by the LaO^+ layer at the interface [53], which coincide with those obtained with the polar catastrophe model. However, such interpretations would fail to explain the results of this paper, where the origin is clearly the polar catastrophe.

V. CONCLUSIONS

In this paper, we have systematically studied the properties of 2DEG at a prototypical ferroelectric interface, $PbTiO_3/SrTiO_3$, finding that, above a critical thickness, the ferroelectric monodomain can be stably sustained by the screening of the depolarization field provided by either a 2DEG or a 2DHG at the interface, depending on the polarization orientation. In this regime, the system possesses a tristable energy landscape in which two polar and metallic states, and one nonpolar and insulating state are accessible. All these results agree very nicely with the predictions of the model described in Ref. [29], including the discontinuous switching of ferroelectricity with thickness. The analysis of the electronic structure of the system has revealed some interesting common features between the electron and hole population distributions in 2DEG and 2DHG, respectively, allowing us to outline some simple rules to predict basic properties of these systems from bulk characteristics of the constituent materials.

The formation of a 2DEG at this very well-known heterostructure may open the door to the design of structurally new, relatively simple, all-oxide, field-effect nonvolatile devices thanks to the retention provided by the spontaneous polarization. The fact that the process is driven by electrostatics means that it is not material-specific, and this idea can be exploited to engineer new functional interfaces or enhance the performance of the device by combining ferroelectric or multiferroic films with, for instance, magnetic substrates.

ACKNOWLEDGMENTS

Computations were performed at the National Supercomputer Center in Tianjin (NSCC-TJ), the Spanish Supercomputer Network (RES), and computational resources at the Donostia International Physics Center. This paper was supported by the National Natural Science Foundation of China (Grants No. 11222218 and No. 11321202), Natural Science Foundation of Zhejiang Province (Grant No. LZ14A020001), the Fundamental Research Funds for the Central Universities, and Spain's Ministry of Economy and Finance (MINECO; Grant No. FIS2012-37549-C05). Atomic configurations were visualized by VESTA [54].

APPENDIX A: EFFECT OF ATOMIC RELAXATIONS ON THE AMOUNT OF FREE CHARGE AND ITS PROFILE

Among the systems studied here, those in which the ferroelectric material possesses a finite polarization have metallic interfaces, regardless of whether they are relaxed or generated using the frozen-phonon scheme. In addition, also in all of them, the amount of free charge accumulated at the interface compensates almost completely for the polarity of the interface. This is the consequence of the huge energy penalty that an unscreened depolarizing field constitutes. The reduction in the electrostatic energy easily compensates for the cost of transferring charge from the valence to the conduction band, and, therefore, for typical materials, free charge accumulates until its value almost reaches that of the polarization.

As discussed in the paper, this phenomenon is driven by electrostatics, and some of the fundamental fingerprints, like the critical thickness or the magnitude of the polarization and free charge, depend mostly on the bulk properties of the ferroelectric material. This is the main reason for the agreement between the relaxed structures and the frozen-phonon analysis. The relaxations of the STO layer play a secondary role in the stabilization of the ferroelectric phase. In general, in the model described by Eq. (3), the influence of the substrate is restricted to the density of states, g, and (possibly) the effective band gap, Δ. Even though, in general, the structural relaxations near the interface can affect the value of Δ, causing disagreements between estimations derived from a

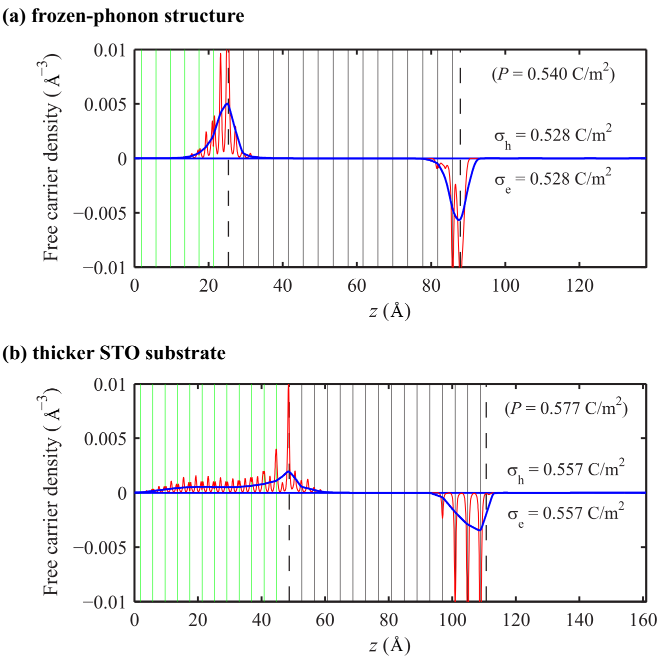

FIG. 8. (Color online) Plane-averaged (red) and macroscopically averaged (blue) profiles of free charge for $m = 16$ interfaces. (a) The frozen-phonon calculation at the local energy minimum of Fig. 2, with upward polarization. (b) The thickness of the STO substrate is 12 unit cells, instead of 6 as in the rest of the article. The positions of interface and surface are indicated by the thick dashed lines, while thin solid lines mark the position of every Ti atom, with green and black for those inside STO and PTO, respectively.

frozen-phonon analysis and the fully relaxed structures, for this particular system, we find that neither the effective band gap of the system nor the DOS at the interface is particularly sensitive to the atomic relaxations, guaranteeing the compatibility of the two methods. Figure 3(b) demonstrates the agreement in the critical thickness and the evolution of the polarization with the thickness of the ferroelectric material. The agreement is also notable in the free charge accumulated at the interface, which amounts to $0.49\,\mathrm{C/m^2}$ [Fig. 4(d)] in the relaxed structure and $0.53\,\mathrm{C/m^2}$ [Fig. 8(a)] in the frozen-phonon one.

On the other hand, the ionic relaxations of the STO layers play a major role in the width of the resulting 2D free-carrier gases. It is evident from the comparison of Fig. 4(d) and Fig. 8(a) that the reduced susceptibility of STO in the frozen-phonon calculations (only the electrons contribute to the material polarizability) results in a stronger confinement of the free charge. In fact, due to the very large susceptibility of STO, the 2DEG or the 2DHG tends to penetrate very deep inside the substrate [47]; this can be appreciated in Fig. 8(b). Additionally, Fig. 8(b) also shows that the values of the stable polarization and free charge, as well as the qualitative aspects of the 2DHG distribution, are well converged for the thickness of 6 unit cells of STO used throughout the paper.

APPENDIX B: POLARIZATION FLUCTUATIONS IN *AB INITIO* FULLY RELAXED STRUCTURES

Due to the shallowness of the energy minimum corresponding to the ferroelectric phase for thicknesses near the transition, any finite value of the force threshold in the atomic relaxations entails some fluctuations in the atomic coordinates and thus in the values of the polarization of the system. The phenomenological model can be used to obtain an estimation of the magnitude of these fluctuations, linking changes in polarization to a threshold in the forces. Assuming that the force tolerance is the same for any atom for a displacement given by a small amplitude of the soft-mode distortion, then a change in energy can be expressed as a line derivative with respect to the amplitude of the soft-mode deformation. Using this premise, the following relation can be found

$$\delta P = \frac{\partial P}{\partial P_\eta}\delta P_\eta = \frac{\partial P}{\partial P_\eta}(-mc)\left(e\sum_{i=1}^{5} Z_i\xi_i \frac{\partial^2 G}{\partial {P_\eta}^2}\right)^{-1} \times \delta\left(\sum_{i=1}^{5} F_i\xi_i\right). \tag{B1}$$

Here, F_i and ξ_i are the force and soft-mode displacement of the ith atom in a perovskites unit cell, P_η is the soft-mode contribution to the polarization, G is the free energy per unit area, c is the out of plane lattice constant of bulk PTO, m is the thickness of the PTO thin film in unit cells, and Z_i is the Born effective charge associated to the ith atom. Using $\delta F_i = 0.025\,\mathrm{eV/Ang}$ as the force threshold used in the *ab initio* optimizations and the curvature of the energy curves at the equilibrium ferroelectric configuration, $\partial^2 G/\partial P^2$, from the fitting of the frozen-phonon calculations, we get the values plotted as error bars in Fig. 3.

APPENDIX C: MAPPING OF FREE-CARRIER DENSITY

The spatial distribution of the free carriers can be mapped in a quantitative way by extending the method used in Ref. [42]. First, the local density of states, $\tilde{\rho}(\mathbf{r},E)$, which is a function of the spatial coordinates $\mathbf{r}$ and the energy E, is computed using the same occupation function (the Fermi-Dirac distribution, f_D, for electrons and $1 - f_D$ for the holes) and smearing temperature as during the self-consistent computation of the one-particle eigenstates. Then, the local density is integrated over an energy window, as indicated by the red dashed lines in Figs. 4(a) and 4(b). It should be noted that by integrating $\tilde{\rho}(\mathbf{r},E)$ for the electrons in the energy window depicted in Fig. 4(a), one obtains contributions from the conduction band near the interface as well as from the valence band near the PTO surface. With an appropriate choice for the energy window, these two contributions are spatially separated while all partially occupied states are included. Then the contribution to the electrons coming from the valence band can be removed, and only the part corresponding to the free electrons is plotted, as shown in Fig. 4(c). The same method is used to plot the free holes in Fig. 4(c) and free electrons and holes in Fig. 4(d).

In this paper, we show the free-carrier densities that are calculated with an energy window spanning from -0.5 eV to 0.5 eV in Figs. 4(c) and 4(d), while integration from -0.6 eV to 0.6 eV gives exactly the same results. This indicates that our choice of the energy window meets the prerequisites mentioned above and should yield meaningful results of the free-carrier density.

[1] H. Y. Hwang, Y. Iwasa, M. Kawasaki, B. Keimer, N. Nagaosa, and Y. Tokura, Nat. Mater. **11**, 103 (2012).
[2] P. Zubko, S. Gariglio, M. Gabay, P. Ghosez, and J.-M. Triscone, Annu. Rev. Condens. Matter Phys. **2**, 141 (2011).
[3] A. Ohtomo and H. Y. Hwang, Nature **427**, 423 (2004).
[4] L. Li, C. Richter, S. Paetel, T. Kopp, J. Mannhart, and R. C. Ashoori, Science **332**, 825 (2011).
[5] A. Brinkman, M. Huijben, M. van Zalk, J. Huijben, U. Zeitler, J. C. Maan, W. G. van der Wiel, G. Rijnders, D. H. A. Blank, and H. Hilgenkamp, Nat. Mater. **6**, 493 (2007).
[6] A. D. Caviglia, S. Gariglio, N. Reyren, D. Jaccard, T. Schneider, M. Gabay, S. Thiel, G. Hammerl, J. Mannhart, and J. M. Triscone, Nature **456**, 624 (2008).
[7] N. Reyren, S. Thiel, A. D. Caviglia, L. F. Kourkoutis, G. Hammerl, C. Richter, C. W. Schneider, T. Kopp, A.-S. Rüetschi, D. Jaccard, M. Gabay, D. A. Muller, J.-M. Triscone, and J. Mannhart, Science **317**, 1196 (2007).
[8] J. A. Bert, B. Kalisky, C. Bell, M. Kim, Y. Hikita, H. Y. Hwang, and K. A. Moler, Nat. Phys. **7**, 767 (2011).
[9] L. Li, C. Richter, J. Mannhart, and R. C. Ashoori, Nat. Phys. **7**, 762 (2011).
[10] C. Cen, S. Thiel, G. Hammerl, C. W. Schneider, K. E. Andersen, C. S. Hellberg, J. Mannhart, and J. Levy, Nat. Mater. **7**, 298 (2008).
[11] C. Cen, S. Thiel, J. Mannhart, and J. Levy, Science **323**, 1026 (2009).
[12] B. Förg, C. Richter, and J. Mannhart, Appl. Phys. Lett. **100**, 053506 (2012).
[13] M. Hosoda, Y. Hikita, H. Y. Hwang, and C. Bell, Appl. Phys. Lett. **103**, 103507 (2013).
[14] M. Boucherit, O. F. Shoron, T. A. Cain, C. A. Jackson, S. Stemmer, and S. Rajan, Appl. Phys. Lett. **102**, 242909 (2013).
[15] Y. Xie, Y. Hikita, C. Bell, and H. Y. Hwang, Nat. Commun. **2**, 494 (2011).
[16] E. Assmann, P. Blaha, R. Laskowski, K. Held, S. Okamoto, and G. Sangiovanni, Phys. Rev. Lett. **110**, 078701 (2013).
[17] H. Liang, L. Cheng, X. Zhai, N. Pan, H. Guo, J. Zhao, H. Zhang, L. Li, X. Zhang, X. Wang, C. Zeng, Z. Zhang, and J. G. Hou, Sci. Rep. **3**, 1975 (2013).
[18] N. Nakagawa, H. Y. Hwang, and D. A. Muller, Nat. Mater. **5**, 204 (2006).
[19] M. Stengel and D. Vanderbilt, Phys. Rev. B **80**, 241103 (2009).
[20] D. G. Schlom and J. Mannhart, Nat. Mater. **10**, 168 (2011).
[21] N. C. Bristowe, P. B. Littlewood, and E. Artacho, Phys. Rev. B **83**, 205405 (2011).
[22] N. C. Bristowe, G. Philippe, P. B. Littlewood, and E. Artacho, J. Phys.: Condens. Matter **26**, 143201 (2014).
[23] L. Yu and A. Zunger, Nat. Commun. **5**, 5118 (2014).
[24] A. Annadi, Q. Zhang, X. Renshaw Wang, N. Tuzla, K. Gopinadhan, W. M. Lü, A. Roy Barman, Z. Q. Liu, A. Srivastava, S. Saha, Y. L. Zhao, S. W. Zeng, S. Dhar, E. Olsson, B. Gu, S. Yunoki, S. Maekawa, H. Hilgenkamp, T. Venkatesan, and Ariando, Nat. Commun. **4**, 1838 (2013).
[25] M. L. Reinle-Schmitt, C. Cancellieri, D. Li, D. Fontaine, M. Medarde, E. Pomjakushina, C. W. Schneider, S. Gariglio, P. Ghosez, J. M. Triscone, and P. R. Willmott, Nat. Commun. **3**, 932 (2012).
[26] V. T. Tra, J.-W. Chen, P.-C. Huang, B.-C. Huang, Y. Cao, C.-H. Yeh, H.-J. Liu, E. A. Eliseev, A. N. Morozovska, J.-Y. Lin, Y.-C. Chen, M.-W. Chu, P.-W. Chiu, Y.-P. Chiu, L.-Q. Chen, C.-L. Wu, and Y.-H. Chu, Adv. Mater. **25**, 3357 (2013).
[27] M. K. Niranjan, Y. Wang, S. S. Jaswal, and E. Y. Tsymbal, Phys. Rev. Lett. **103**, 016804 (2009).
[28] K. D. Fredrickson and A. A. Demkov, Phys. Rev. B **91**, 115126 (2015).
[29] P. Aguado-Puente, N. C. Bristowe, B. Yin, R. Shirasawa, P. Ghosez, P. B. Littlewood, and E. Artacho, Phys. Rev. B **92**, 035438 (2015).
[30] C. Thompson, C. M. Foster, J. A. Eastman, and G. B. Stephenson, Appl. Phys. Lett. **71**, 3516 (1997).
[31] M. J. Bedzyk, A. Kazimirov, D. L. Marasco, T. L. Lee, C. M. Foster, G. R. Bai, P. F. Lyman, and D. T. Keane, Phys. Rev. B **61**, R7873 (2000).
[32] S. K. Streiffer, J. A. Eastman, D. D. Fong, C. Thompson, A. Munkholm, M. V. Ramana Murty, O. Auciello, G. R. Bai, and G. B. Stephenson, Phys. Rev. Lett. **89**, 067601 (2002).
[33] D. D. Fong, G. B. Stephenson, S. K. Streiffer, J. A. Eastman, O. Auciello, P. H. Fuoss, and C. Thompson, Science **304**, 1650 (2004).
[34] C. Thompson, D. D. Fong, R. V. Wang, F. Jiang, S. K. Streiffer, K. Latifi, J. A. Eastman, P. H. Fuoss, and G. B. Stephenson, Appl. Phys. Lett. **93**, 182901 (2008).
[35] D. D. Fong, C. Cionca, Y. Yacoby, G. B. Stephenson, J. A. Eastman, P. H. Fuoss, S. K. Streiffer, C. Thompson, R. Clarke, R. Pindak, and E. A. Stern, Phys. Rev. B **71**, 144112 (2005).
[36] J. M. Soler, E. Artacho, J. D. Gale, A. García, J. Junquera, P. Ordejón, and D. Sánchez-Portal, J. Phys.: Condens. Matter **14**, 2745 (2002).
[37] L. Kleinman and D. M. Bylander, Phys. Rev. Lett. **48**, 1425 (1982).
[38] N. Troullier and J. L. Martins, Phys. Rev. B **43**, 1993 (1991).
[39] J. Junquera, M. Zimmer, P. Ordejón, and P. Ghosez, Phys. Rev. B **67**, 155327 (2003).
[40] H. J. Monkhorst and J. D. Pack, Phys. Rev. B **13**, 5188 (1976).
[41] J. Moreno and J. M. Soler, Phys. Rev. B **45**, 13891 (1992).
[42] M. Stengel, P. Aguado-Puente, N. A. Spaldin, and J. Junquera, Phys. Rev. B **83**, 235112 (2011).
[43] B. Meyer and D. Vanderbilt, Phys. Rev. B **63**, 205426 (2001).
[44] M. Stengel, C. J. Fennie, and P. Ghosez, Phys. Rev. B **86**, 094112 (2012).
[45] A. K. Tagantsev, Ferroelectrics **69**, 321 (1986).
[46] J. Javier, H. C. Morrel, and M. R. Karin, J. Phys.: Condens. Matter **19**, 213203 (2007).
[47] M. Stengel, Phys. Rev. Lett. **106**, 136803 (2011).
[48] N. C. Bristowe, E. Artacho, and P. B. Littlewood, Phys. Rev. B **80**, 045425 (2009).
[49] Z. S. Popović, S. Satpathy, and R. M. Martin, Phys. Rev. Lett. **101**, 256801 (2008).
[50] P. Delugas, A. Filippetti, V. Fiorentini, D. I. Bilc, D. Fontaine, and P. Ghosez, Phys. Rev. Lett. **106**, 166807 (2011).
[51] H. Chen and N. Umezawa, Phys. Rev. B **90**, 035202 (2014).
[52] E. V. Chenskii, Fiz. Tverd. Tela **14**, 2241 (1972) [Sov. Phys. Solid State **14**, 1940 (1973)].
[53] A. Janotti, L. Bjaalie, L. Gordon, and C. G. Van de Walle, Phys. Rev. B **86**, 241108 (2012).
[54] K. Momma and F. Izumi, J. Appl. Crystallogr. **44**, 1272 (2011).